Wind and Structures, *Vol. 19, No. 4 (2014) 421-441*
DOI: http://dx.doi.org/10.12989/was.2014.19.4.421

Wind-excited stochastic vibration of long-span bridge considering wind field parameters during typhoon landfall

Yaojun Ge[a] and Lin Zhao[*]

State Key Laboratory for Disaster Reduction in Civil Engineering, Tongji University, Shanghai, China

(Received May 30, 2014, Revised August 20, 2014, Accepted August 30, 2014)

Abstract. With the assistance of typhoon field data at aerial elevation level observed by meteorological satellites and wind velocity and direction records nearby the ground gathered in Guangzhou Weather Station between 1985 and 2001, some key wind field parameters under typhoon climate in Guangzhou region were calibrated based on Monte-Carlo stochastic algorithm and Meng's typhoon numerical model. By using Peak Over Threshold method (POT) and Generalized Pareto Distribution (GPD), Wind field characteristics during typhoons for various return periods in several typical engineering fields were predicted, showing that some distribution rules in relation to gradient height of atmosphere boundary layer, power-law component of wind profile, gust factor and extreme wind velocity at 1-3s time interval are obviously different from corresponding items in Chinese wind load Codes. In order to evaluate the influence of typhoon field parameters on long-span flexible bridges, 1:100 reduced-scale wind field of type B terrain was re-illustrated under typhoon and normal conditions utilizing passive turbulence generators in TJ-3 wind tunnel, and wind-induced performance tests of aero-elastic model of long-span Guangzhou Xinguang arch bridge were carried out as well. Furthermore, aerodynamic admittance function about lattice cross section in mid-span arch lib under the condition of higher turbulence intensity of typhoon field was identified via using high-frequency force-measured balance. Based on identified aerodynamic admittance expressions, Wind-induced stochastic vibration of Xinguang arch bridge under typhoon and normal climates was calculated and compared, considering structural geometrical non-linearity, stochastic wind attack angle effects, etc. Thus, the aerodynamic response characteristics under typhoon and normal conditions can be illustrated and checked, which are of satisfactory response results for different oncoming wind velocities with resemblance to those wind tunnel testing data under the two types of climate modes.

Keywords: wind-induced vibration; long-span bridge; typhoon; wind tunnel test; numerical simulation

1. Introduction

At present, wind-induced vibration theory and wind-resistant structural design usually base themselves on normal climate, in other words, non-typhoon condition, such as monsoon and cold snap. Wind field parameters, including gust factor, profiles concerning mean wind and turbulent intensity, turbulent integral scale, wind spectrum equation etc., are mainly related to monsoon condition in non-typhoon regions. However, it's well known that many high-rise buildings and

*Corresponding author, Associate Professor, E-mail: zhaolin@tongji.edu.cn
[a] Professor, E-mail: yaojunge@tongji.edu.cn

http://www.techno-press.org/?journal=was&subpage=8 ISSN: 1226-6116 (Print), 1598-6225 (Online)

long-span bridges located in typhoon-prone coastline areas are very sensitive to wind dynamic action through some investigation about the on-site measurements, wind tunnel tests and numerical calculation (Xu and Zhan 2001, Li *et al*. 2002, Campbell *et al*. 2005, Li *et al*. 2004, 2008, Zhao *et al*. 2013, Ma *et al*. 2013), and wind environment parameters and wind-induced vibration characteristics during typhoons also differ from normal climates (Zhu 2002, Zhu *et al*. 2012). The indication is that turbulent intensity and gust factor nearby the ground could be larger than predefined values from wind loading Codes, the slope ratios of mean wind profile under typhoon are less than corresponding values in normal condition (Mikitiuk and Isyumov 1994, Amano *et al*. 1999, John and Chou 2001). As expected, design wind loading and wind-excited responses of flexible structures are also quite different between the two types of climate modes (Pande *et al*. 2002, Zhu 2002, Eamon *et al*. 2007). Despite the western Pacific Ocean region, including southeastern coast of China and most of Korea and Japan, are seriously affected by strong typhoons with the highest recorded wind velocities, investigations about typhoon dynamic action on high rise buildings and long-span bridges are so deficient that it has posed a thorny problem to the structural engineers.

2. Typhoon field parameters

Design wind loads for structures in coastal areas are usually governed by strong typhoons. In order to reasonably determine design wind velocities for these structures by means of standard statistical techniques, at least several decades of annual or lunar extreme wind observations would be needed at the proposed construction site. However, such data bases, which would allow reconstruction of the wind climate caused by typhoons, rarely exist because typhoons are relatively small in size and infrequent in occurrence. An alternative approach to formulate design wind loads in areas which are dominated by tropical cyclones was first suggested by Russell (1971) and then developed by a number of researchers (Meng and Matsui 1995, 1997, Vickery and Skerlj 2000, etc.). The advantage of such approach is that multiple time histories of tropical cyclones in a given locality can be created by computer simulation with the employment of the so-called "Monte Carlo" method. These are then applied to provide estimates of extreme winds over what are, in effect, long periods of time. Within the simulation, probability distributions of tropical cyclone parameters (such as annual occurrence rate, moving paths, translation velocity, radius of maximum winds, central pressure difference and decay rate after landfall) are first determined from the observation data, followed by prediction of wind field associated with them.

Xinguang long-span arch bridge (see Figs. 1 and 2), located in vicinity of Guangzhou downtown across the Zhu River, a typical typhoon-prone coastal area, was selected to conduct case study on aerodynamic action under strong typhoons. A lot of macroscopical or “large-scale” parameters about tropical cyclones from meteorological satellites during typhoon movements that had unquestionably affected construction fields over the past 50-odd years, were obtained from the Chinese Meteorological Bureau. Totally, 165 typhoons moving tracks across Guangzhou region from 1949 to 2001 and local geographical map are illustrated in Figs. 3(a) and 3(b). Wind velocity and direction records nearby the ground surface continuously measured in the Guangzhou Weather Station neighbouring the construction fields (beeline distance less than 20km, showed in Fig.3(c)) for the past 25-35 years (1985-2001) were also collected.

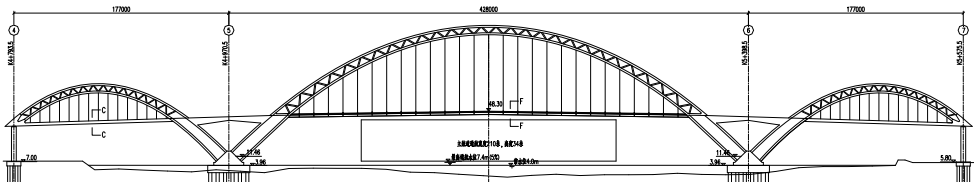

Fig. 1 General arrangement drawing of the main bridge of Xinguang Bridge (Unit: mm)

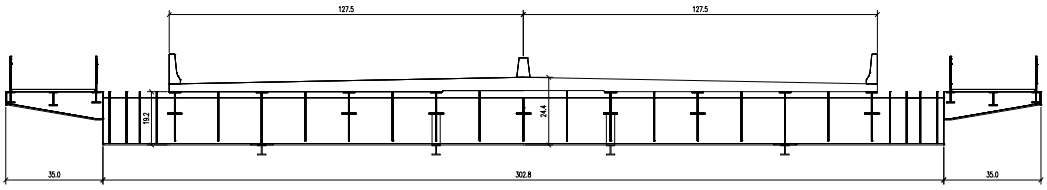

Fig. 2 Cross section of main girder of Xinguang Bridge (Unit: 100 mm)

(a) From 1949 to 1984 , totally 106 tracks

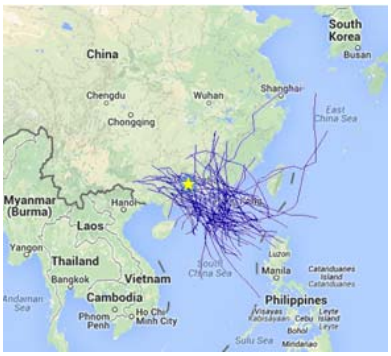

(b) From 1985 to 2001, totally 59 tracks

(c) Geographical position about Xinguang Bridge and weather station

Fig. 3 Moving tracks of 165 typhoons and geographical map

Table 1 Definition of field stochastic parameters during typhoons

Var./Unit	Coefficient of variation	Upper /Lower limitation	Distribution type
ΔP (kPa)	0.2		Normal
R_m (km)	0.4		Normal
c(m/s)	0.5		Normal
β		1.0 ~ 2.5	Uniform
L_a (°)	0.067		Normal
L_o (°)	0.0154		Normal
z_0 (B)		0.01 ~ 0. 1	Uniform
z_0 (C)		0.1 ~ 0. 4	Uniform

Definition of wind field stochastic parameters during typhoons are listed in Table 1 as well, in which ΔP is central pressure difference between periphery pressure and central (minimum) pressure, R_m is radius of maximum winds, c is translation velocity of typhoon, β is horizontal pressure profile constant, L_a and L_o are latitude and longitude of typhoon center, z_0(B) and z_0(C) are ground roughness length for standard Type B and C terrain, respectively. Some key parameters, which have larger sensitivity indices calculated by Finite-difference method, could be calibrated by on-site measurement data directly or indirectly. With the aid of Monte-Carlo stochastic simulation methods and the Meng's typhoon numerical model (Meng *et al*. 1995), the design wind parameters for typical terrains could be predicted by using Peak Over Threshold method and Generalized Pareto Distribution. In the process of Monte-Carlo simulation, some basic statistical relation involving typhoon field parameters are introduced and compared, including R_m and ΔP expressions fitted by Yasui *et al*. (2001) shown as Eq. (1)

$$E(R_m) = 2.06 \times 10^4 \Delta P^{-1.27} \tag{1}$$

in which, $E()$ means average value of R_m. Horizontal pressure profile coefficient β can be defined as the function of R_m and ΔP. In this investigation, Jakobsen equation shown as Eqs. 2(a) and 2(b) (Jakobsen *et al*. 2004) and FEMA expression (FEMA, 2003) proposed by U.S. Federal Emergency Management Agency listed as Eq. (3) are utilized

$$\beta = \frac{e}{r_2^2} \frac{\rho_A}{[100]\Delta P} (V_{\max})^2 \tag{2a}$$

$$V_{\max} = \left[\frac{1}{3.6}\right] K_p (\Delta P)^{\alpha} \tag{2b}$$

$$\beta = 1.38 + 0.00184\Delta P - 0.00309 R_{\max} \tag{3}$$

in which, e=2.71828, r_2=1.05, ρ_A=1.15kg/m3, K_p and β are fitted parameters, K_p=12.36, α=0.73. For the sake of brevity, more details can be referred to in some journal papers (Ge *et al*. 2002, Zhao *et al*. 2005, 2007, 2013). Meanwhile, the wind field parameters of the construction field under normal climate can be determined from basic wind pressure map or probability statistical

results from nearby meteorological stations.

Since ground roughness length z_0 and horizontal pressure profile constant β have larger sensitive indices about design wind velocity in the domain of typhoon, the randomness about z_0 and β could not be ignored safely. Some calibration steps are required in light of on-site measurement data during typhoons. In order to estimate error, three standards, as Eqs. (4)-(6), are accordingly defined to evaluate Monte-Carlo typhoon simulation results and those measured in Guangzhou Meteorological Station

$$D_1 = \left(\frac{1}{n} \sum_{i=1}^{n} \left(\left(v_{c,i} \quad v_{o,i} \right) / v_{o,i} \right)^2 \right)^{0.5} \tag{4}$$

$$D_2 = \frac{1}{n} \sum_{i=1}^{n} \left(\left(v_{c,i} \quad v_{o,i} \right) / v_{o,i} \right) \tag{5}$$

$$D_3 = \left(v_{c,N} - v_{o,N} \right) / v_{o,N} \tag{6}$$

in which, n is typhoon occurrence times recorded in the meteorological station, $v_{o,i}$ is the i^{th} observed maximal wind velocity, $v_{c,i}$ is the ith calculated value, $v_{o,N}$ is the observed maximal wind velocity for N years return period, $v_{c,N}$ is the predicted result from Monte-Carlo method for N years return period.

For the field condition about Guangzhou Meteorological Station, considering historical transition of the adjacent buildings around the weather station, the calibration process can be divided into two stages: namely, before 1984, while β lies in 1.00-2.50 and z_0 is equal to 0.125 close to standard B type terrain, then after 1985, while β lies in 1.00-2.50 and z_0 is equal to 0.250 close to standard C type terrain, the best analysis result can be obtained based on stochastic typhoon gradualness comparison standard (see Eqs. (4)-(6)). Some on-spot observed records about wind velocity procedures from 1985 to 2001 are also collected. In order to take into account more observed typhoon procedures and avoid the disturbance from other climate modes, such as monsoon and cold current, the wind velocity lower limitation should larger than wind force eight (namely 15 m/s at 10min time interval). So, totally 39 typhoon records were selected, in which the minimal wind velocity is 15.6m/s, and maximal wind velocity is 29.0m/s. Though, all the records are less than the stand strong typhoon records, the records can show the characteristics during the decay stage in Northwestern Pacific Ocean. In Fig. 4, comparison between measured and simulated wind velocity in Guangzhou Meteorological Station in 39 strong typhoon records with a height of 10 m from the ground is demonstrated, and satisfactory agreement between them is almost the total. Mean square departure D_1 is 23.0%-33.0%, mean departure D_2 is -1.6%-1.0%, while mean departure about various return periods D_3 can also be limited in 5.0%-14.0%.

Using the above optimized field parameters, some wind distribution characteristics about gradient height, mean and instantaneous velocity profile in typhoon boundary layer, can be simulated with improved accuracy, in which modified formulas with regard to turbulent intensity and gust factor, original suggested by Sharma (Sharma and Richards 1999) from Australia wind loading Code AS1170.2-1989, are adopted and can be written as

$$I_u(TC) = \alpha \times I_u(Non-TC) \tag{7}$$

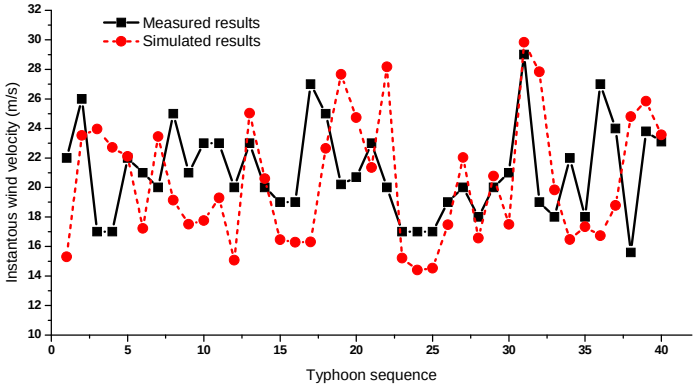

Fig. 4 Comparison between measured and simulated wind velocity in Guangzhou Meteorological Station

$$\gamma_G(TC) = 1 + 3.7 I_u(TC) \tag{8}$$

in which *TC* indicates the domain of typhoon, *Non-TC* is the domain of non-typhoon, I_u is turbulent intensity, γ_G is gust factor, and for Type A-D terrains, modification coefficient α is 1.60, 1.48, 1.36, 1.24, respectively.

Wind field parameters regarding Xinguang Bridge construction field through no less than 104 Monte-Carlo stochastic simulations are listed in Table 2. As expected, two types of climate modes vary in characteristics, and in fact, for different height from the ground surface to the gradient height, they dominate design wind velocity, respectively. Some conclusions can be drawn that gradient height under typhoon is usually lower than normal climate with gust factor featuring reverse tendency. From the height of 10 m to 55 m (average main girder height), design mean wind velocity is governed by normal climate. In the case of Type A terrain, instantaneous wind velocity of normal climate at the height of average main girder is higher than 13.3% in typhoon climate, while in Type B terrain, instantaneous wind velocity of typhoon climate at the height of average main girder is greater than 13.1% in normal condition. In a word, the instantaneous wind velocity under two types of terrains dominates design wind loads, respectively.

Table 2 Wind field parameters for A and B terrain (100y return period)

Type terrain		A		B	
Climate mode		Normal	Typhoon	Normal	Typhoon
Power exponent of profile		0.12	0.062	0.16	0.08
Gradient height (m)		300.0	100.0	350.0	150
10m height	Gust factor	1.38	1.83	1.38	1.93
	Mean velocity (m/s)	39.6	32.5	33.4	34.9
	Instantaneous velocity (m/s)	54.6	59.5	46.1	67.4
Average main girder height (55 m)	Gust factor	1.38	1.59	1.38	1.71
	Mean velocity (m/s)	48.6	36.1	43.9	40.0
	Instantaneous velocity (m/s)	67.1	57.4	60.5	68.4

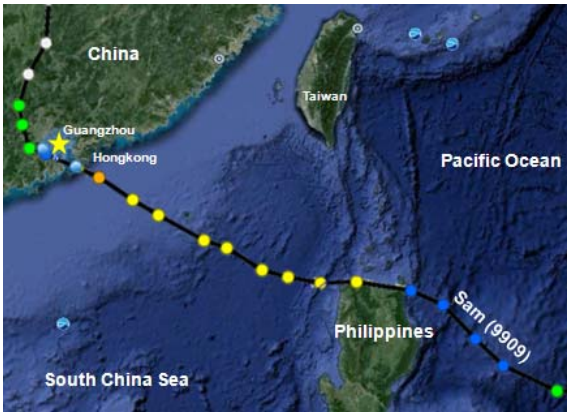

Fig. 5 Sam (1999) typhoon moving track across Guangzhou region

Wind spectrum function under normal climate can be referred to Chinese Codes, in which Simiu and Panofsky functions are selected as horizontal and vertical wind spectrum, respectively, shown as the below in Eqs. (9) and (10).

$$\text{Simiu spectrum:} \quad \frac{nS_u(n)}{u_*^2} = \frac{200f}{(1+50f)^{5/3}} \tag{9}$$

$$\text{Panofsky spectrum:} \quad \frac{nS_w(n)}{u_*^2} = \frac{6f}{(1+4f)^2} \tag{10}$$

in which $S(n)$ is horizontal or vertical power spectrum function, n is frequency component about fluctuating wind velocity history, $f=nz/U(z)$ is reduced frequency, u^* is the friction velocity at the surface.

The definition about spatial coherence function is also given as below (see Eq. (11)). For j direction, in which j means x, y or z coordinate, so for the two spatial points with the distance r_i in which i means u, v or w fluctuation component of wind, $U(z)$ is the mean wind velocity at the height of z. Spatial correlation function Coh_{ij}(f) could be expressed as

$$Coh_{ij}(f) = \exp\left(-\lambda_{ij}\frac{fr_j}{U_Z}\right) \tag{11}$$

in which λ_{ij} is non-dimensional decay factor, lies between 7-20.

With a view to describing the fluctuation of stochastic wind during typhoons, fitted spectrum expression of Sam strong typhoon (Fig. 5 thick solid line), which severely affected Guangzhou region in 1999, is defined as input wind spectrum as

$$\frac{nS(n)}{u_*^2} = \frac{a\ f}{(1+bf^{1/m})^{cm}} \quad \text{c=5/3} \tag{12}$$

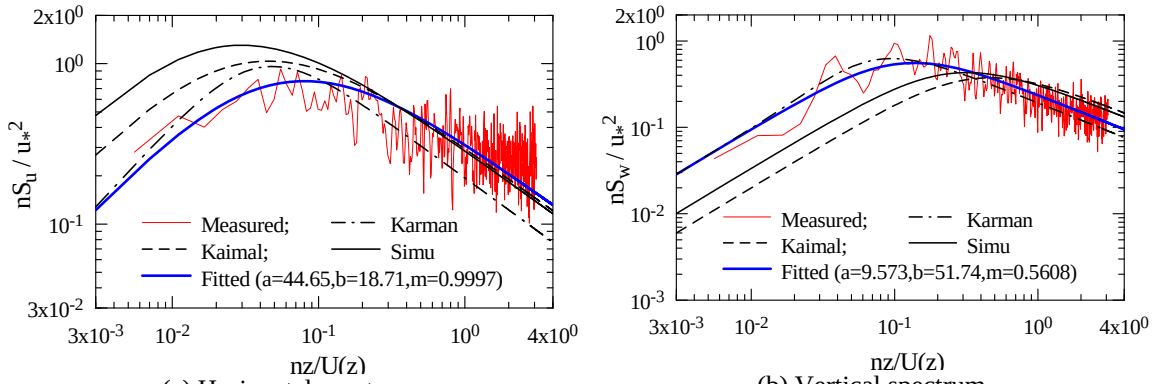

(a) Horizontal spectrum (b) Vertical spectrum

Fig. 6 Fitting power spectrum expressions about Sam (1999) strong typhoon

where a,b,c and m are fitting parameters. There are distinct changing tendency regarding reduced power spectrum density distribution between normal and typhoon climates, especially, while reduced frequency f is less than 0.2, indicating that wind-induced vibration of flexible structures would differ to a large extent in the lower reduced frequency scope for under types of climates, illustrated in Fig. 6 (Zhu 2002).

3. Aerodynamic loading

The aerodynamic forces acting on 2-D line-like cross-section of bridge girder or arch can be formulated as

$$M\ddot{X} + C\dot{X} + KX = F_G + F_{st} + F_b + F_{se} \tag{13}$$

in which M, C, and K are mass, damping and stiffness matrix. X is displacement vector, including lateral, vertical and torsional movements. F_G, F_{st}, F_b and F_{se} are gravity, static wind force, stochastic buffeting force and self-excited aerodynamic force, respectively.

3.1 Self-excited force

The motion-dependent aero-elastic forces distributed on unit span of bridge girder are expressed as a linear function of nodal displacement and nodal velocity (Scanlan 1978, Jain *et al.* 1996). The effect of self-excited force, describing complicated interference between moving cross-section and atmospherical flow, can be equivalently treated as combination about aerodynamic stiffness and aerodynamic damping (Namini 1991), like this

$$F_{se} = K_{se}X + C_{se}\dot{X} \tag{14}$$

$$M\ddot{X} + \left(C - C_{se}\right)\dot{X} + \left(K - K_{se}\right)X = F_G + F_{st} + F_b \tag{15}$$

in which aerodynamic stiffness and damping matrix can be expressed as

$$\left[K_{se}^{i}\right]_l = \rho U^2 L_e K_{cr}^2 \begin{bmatrix} 0 & 0 & 0 & 0 & 0 & 0 \\ 0 & H_4 & H_6 & BH_3 & 0 & 0 \\ 0 & P_6 & P_4 & BP_3 & 0 & 0 \\ 0 & BA_4 & BA_6 & B^2 A_3 & 0 & 0 \\ 0 & 0 & 0 & 0 & 0 & 0 \\ 0 & 0 & 0 & 0 & 0 & 0 \end{bmatrix} \tag{16}$$

$$\left[C_{se}^{i}\right]_l = \rho U B L_e K_{cr} \begin{bmatrix} 0 & 0 & 0 & 0 & 0 & 0 \\ 0 & H_1 & H_5 & BH_2 & 0 & 0 \\ 0 & P_5 & P_1 & BP_2 & 0 & 0 \\ 0 & BA_1 & BA_5 & B^2 A_2 & 0 & 0 \\ 0 & 0 & 0 & 0 & 0 & 0 \\ 0 & 0 & 0 & 0 & 0 & 0 \end{bmatrix} \tag{17}$$

where ρ is air density, U is oncoming mean wind velocity, K_{cr} is reduced frequency matrix, B and L_e are width and length items of moving cross-section, P_i^*, H_i^* and A_i^* are flutter derivatives for lateral, vertical and torsional movements. For the sake of brevity, some detailed derived steps are ignored. The commercial software ANSYS has provided a kind of special element types, MATRIX27, which could be defined by customers so that we can utilize this convenience to realize the above mentioned aerodynamic stiffness and damping effects through the additory couple MATRIX27 elements at the end of realistic elements to describe the self-excited aerodynamic force effect (Fig. 7).

3.2 Buffeting force

At present, the wind-induced stochastic buffeting analysis is still based on quasi-steady theory considering admittance function modification. Traditional Liepmann's approximation to Sears function derived from thin plate and streamline aerofoil, or so-called maximal value 1.0 approximated as the possible upper limitation are usually applied in practical engineering application. In this investigation, the wind induced lateral response have prominent role in the wind excited performance of long-span arch bridge, especially for flexible arch lib, so more attentions about admittance function identification and application is only focused on along wind aerodynamic loads. The buffeting force expressions in time-domain and frequency-domain about cross section (i.e., drag force) can be written as

$$D_b(t) = 1/2\,\rho U^2 B\left(2C_D \chi_{Du} \frac{u(t)}{U} + (C_D' - C_L)\chi_{Dw} \frac{w(t)}{U}\right) \tag{18}$$

$$S_D(\omega) = \rho^2 U^2 B^2 \left(C_D^2(\alpha)\left|\chi_{Du}\right|^2 S_u(\omega) + 1/4\left(C_D'(\alpha) - C_L(\alpha)\right)^2 \left|\chi_{Dw}\right|^2 S_w(\omega)\right) \tag{19}$$

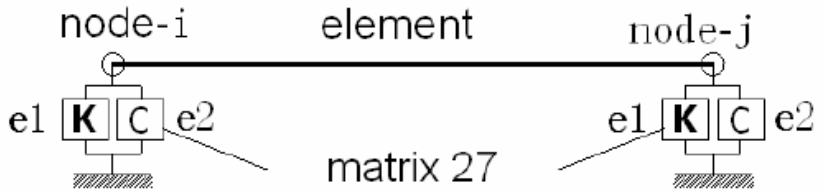

Fig. 7 Additory aerodynamic MATRIX27 element on structural element

in which D is drag buffeting force in the lateral movement direction, C means static aerodynamic coefficient, C' defines the derivative to wind attack angle, χ represents aerodynamic admittance function, u and w are horizontal and vertical fluctuating wind components.

Sears function was originally derived from thin aerofoil in isotropy flow field, but most of bridge cross sections have the characteristics of blunt body, more or less, so we have to face the doubt concerning whether or not the Sears function deriving from streamline structures is still suitable for blunt parts in long-span bridge structures. Considering the absence of time-domain admittance formula, an alternative method can be used: firstly, modify the wind spectrum expressions $S_u(\omega)$ and $S_w(\omega)$ by multiplying admittance function in frequency-domain, that are $|\chi_{Du}|^2 S_u(\omega)$ and $|\chi_{Dw}|^2 S_w(\omega)$; then, change modified wind spectrum into time history using harmonic wave combination technique. Stochastic wind history along the arch lib and main girder in Xinguang Bridge are numerical simulated. Based on the requirement from Wind Loading Codes from various countries, the correlation between longitude and vertical wind component is assumed to be non-correlated, and coherence function about different spatial points for longitude or vertical direction are set to follow the relationship like. In order to simulate spatial points stochastic wind histories simultaneously, improved Deodatis algorithm are used (Deodatis 1996, Ding *et al*. 2011), which is the commonly-used algorithm and can guarantee the simultaneous simulation about stochastic process.

For the convenience of usability, equivalent expression (drag item) about multi-components admittance function have been proposed as

$$|\phi_{DD}(K)|^2 = \frac{4C_D^2(\alpha)|\chi_{Du}|^2 S_u(K) + (C_D' - C_L)^2 |\chi_{Dw}|^2 S_w(K)}{\left(4C_D^2(\alpha)S_u(K) + C_D'^2 S_w(K)\right)} \tag{20}$$

in which, $|\phi_{DD}(K)|^2$ is equivalent admittance in drag force direction, $|\chi_{Du}|^2$ and $|\chi_{Dw}|^2$ define the crisscross admittance components regarding u and w direction. So, the drag spectrum can be changed into the simplified expression

$$S_D(\omega) = \rho^2 U^2 B^2 |\phi_{DD}(K)|^2 \left(C_D^2(\alpha)S_u(\omega) + 1/4\left(C_D'(\alpha) - C_L(\alpha)\right)^2 S_w(\omega)\right) \tag{21}$$

The $|\phi_{DD}(K)|^2$ can be identified using high-frequency force-measured balance and be fitted using double logarithm coordinate third-order multinomial as

$$\log_{10}\left(F(\omega)\right)=\sum_{i=0}^{3}\left(a_i\log_{10}{}^{i}\left(\omega B/U\right)\right) \tag{22}$$

where a_i are fitting parameters, ω defines circular frequency. The goal spectrum $|\phi_{DD}(K)|^2 S_u(\omega)$ and $|\phi_{DD}(K)|^2 S_w(\omega)$, which are modified with equivalent admittance function, can be changed into fluctuating wind history by using harmonic wave combination method, and the stochastic wind time-domain signal $\chi_{Du}u(t)$ and $\chi_{Dw}w(t)$ can be finally obtained. In fact, the phasic angle information about oncoming wind dynamic action are more or less ignored in the above conversion process from fluctuating wind to aerodynamic load, however, the statistical results of wind induced response are still of rationality.

4. Case study of engineering application

4.1 Flow condition and aerodynamic parameters

In this study, Xinguang long-span steel-lattice arch bridge, located in southeastern coast of China, belonging to typical typhoon-prone regions, is selected as numerical examples, shown as Figs. 1-3. The basic design and aerodynamic parameters concerning Xinguang Bridge are presented in Table 3, and the main natural frequencies and mode shapes is also listed in Table 4. It is clear that the several dominated modes with lower frequency values come from the contribution of main arch movement. The static wind coefficient and aerodynamic derivatives for various wind velocities and wind attack angles are identified basing on 2-D cross section wind tunnel tests like other most commonly-used wind-resistance procedures, and the full-scale aeroelastic model with 1:100 reduced-scale ratio was also designed and manufactured in TJ-3 wind tunnel (Fig. 8).

Table 3 Basic parameters about Xinguang arch bridge

Structural type		428 m steel-lattice arch bridge			
Average girder height (m)		55.0			
Main arch size in mid-span		Width (m)		Height (m)	
		30.7		7.6	
Vibration type		Vertical	Lateral	Torsion	
Dynamic characteristics	Frequency (Hz)	0.521	0.218	1.155	
	Damping ratio	4.2‰	6.4‰		
Static aerodynamic items		Lift force	Drag force	Moment	
0°attack angle	Mean value	-0.002	0.261	0.001	
	Slope ratio	0.126	-0.010	-0.026	
Self-excited aerodynamic items		Lift force		Drag force	
0°attach angle		H1	H4	P1	P4
Main derives (normal)		-1.462	-2.235	1.009	-0.560
Main derives (typhoon)		-1.450	-1.757	1.112	-0.314

Table 4 Some natural frequencies of bridge and its mode shapes

No.	Fre. /Hz	Mode shape
1	0.218	First order symmetric lateral bending of main arch
2	0.417	Second order antisymmetric lateral bending of main arch
3	0.418	First order symmetric lateral bending of main girder
4	0.521	First order symmetric vertical bending of main girder and arch
5	0.691	Second order antisymmetric vertical bending of main girder and arch
6	1.155	First order symmetric torsion of main girder
7	1.169	Second order antisymmetric torsion of main girder

Fig. 8 1:100 aeroelastic model of Xinguang Bridge in TJ-3 wind tunnel

To investigate the effects of climate mode on wind-induced vibration quantitatively, the case study about Xinguang Bridge are therefore carried out. Firstly, the passive turbulent generators, such as triangle and rectangle spine and various roughness blocks are used in TJ-3 wind tunnel to re-illustrate the 1:100 reduced-scale wind fields about Type B terrain under normal and typhoon conditions (see Fig. 9), and mean wind velocity and turbulent intensity profile are in good agreement with Codes definition during normal climate and Monte-Carlo predicted values about typhoon modes (see Table 2, Figs. 10 and 11).

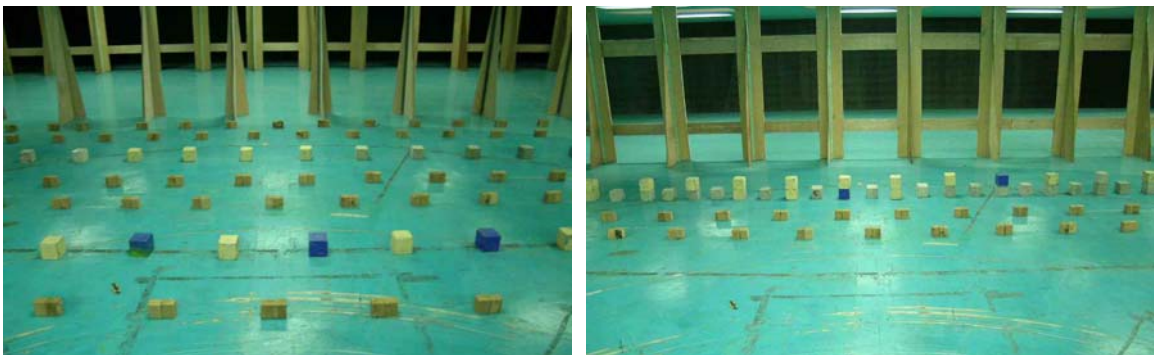

(a) Normal climate wind field, Type B (b) Typhoon climate wind field, Type B

Fig. 9 Passive turbulent generators in TJ-3 wind tunnel

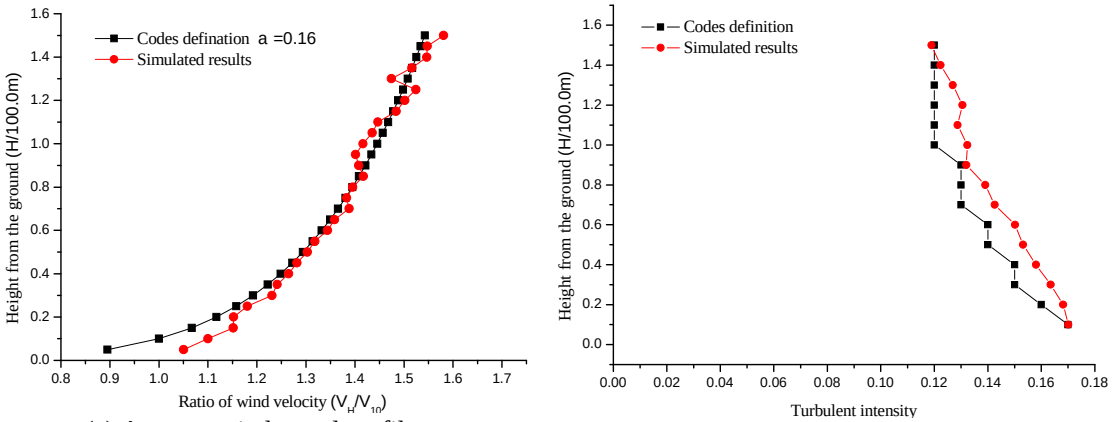

(a) Average wind speed profile (b) Turbulence instensity profile

Fig. 10 Wind profiles under normal climate

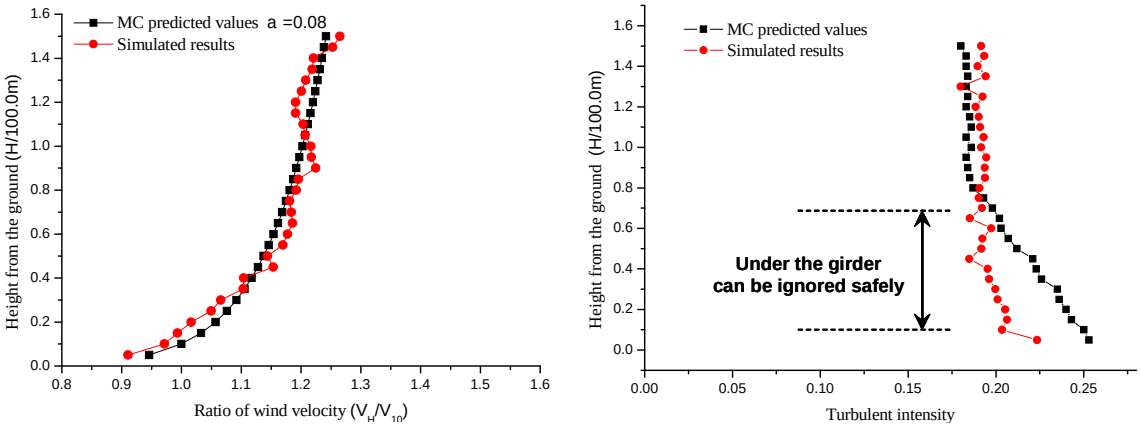

(a) Average wind speed profile (b) Turbulence instensity profile

Fig. 11 Wind profiles under typhoon climate

The wind spectrum in TJ-3 under normal and typhoon conditions were also measured and compared with standard spectrum suggested by Chinese wind loading Codes. Usually, the turbulence intensity under typhoon condition is larger than those under normal climate for various heights from the ground. The same tendencies along the frequency coordinate were reillustrated in Figs. 12 and 13. For the normal condition, there is obviously coincidence between measured spectrum and standard spectrum (Simiu and Panofsky spectrum, see Eqs. (9) and (10)). However, for the typhoon condition, though integral value about non-dimensional power spectrum intensity function along the reduced frequency coordinate has the same value that is 1.0 like those under normal condition, another changing tendencies show the wind field characteristics during typhoon climate. It is easily found that spectrum intensity is lower than corresponding value in the lower frequency of normal wind field, and in the higher frequency scope, spectrum intensity values of typhoon field are larger than those of normal field.

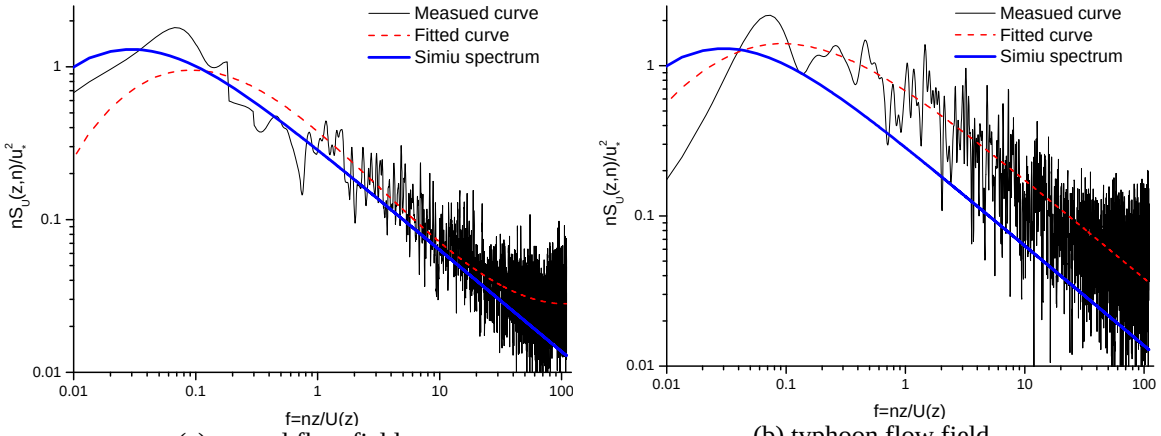

(a) normal flow field (b) typhoon flow field

Fig. 12 Longitude spectrum comparison under normal and climate conditions

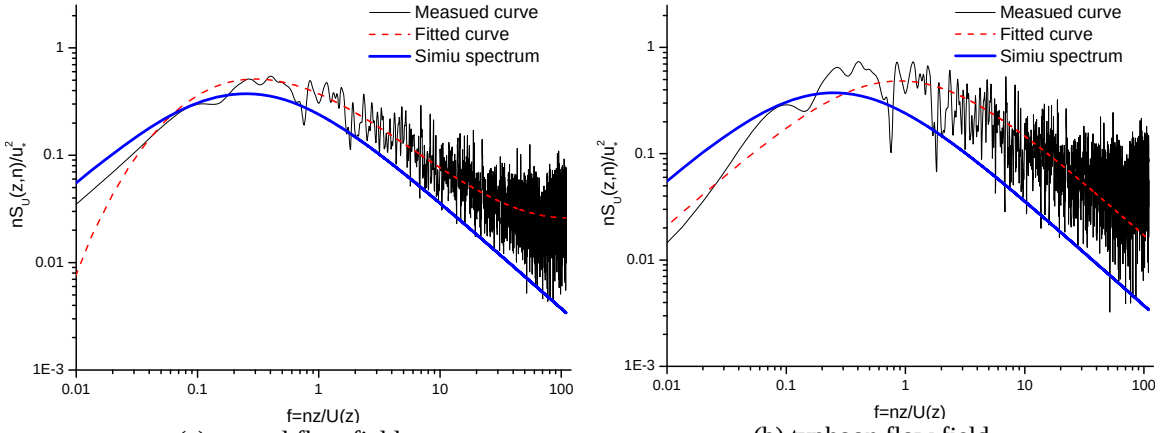

(a) normal flow field (b) typhoon flow field

Fig. 13 vertical spectrum comparison under normal and climate conditions

Then, the wind-excited performance about Xinguang aeroelastic model was measured under typhoon and normal climate modes. In order to improve the precision of numerical simulation, the equivalent admittance function of main arch lib section (see Fig. 14) are also identified using dynamic force measured testing system (see Fig. 15) and recognized algorithm(see Eqs. (20-22)). The fitted parameters defined in Eq. (22) are a_0 =-0.904, a_1 =-0.946, a_2 =-0.029, a_3 =0.056 for normal condition, and a_0 =-0.678, a_1 =-1.436, a_2 =-1.321, a_3 =-0.324 for typhoon condition. It's obvious that the realistic admittance function about arch rib section are different from Sears function to some extent (see Fig. 16, blue thick solid line), showing the characteristics of dependence on the oncoming turbulent intensity for two types of climate modes.

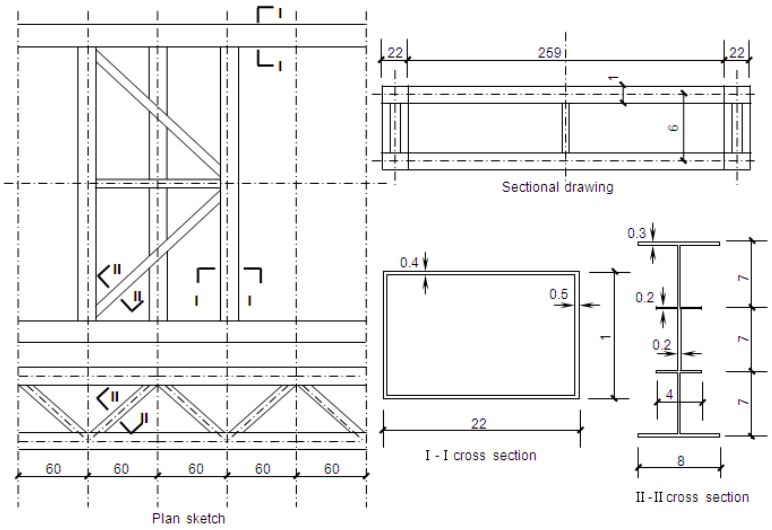

Fig. 14 Wind tunnel model of cross section of main arch lib (Unit:mm)

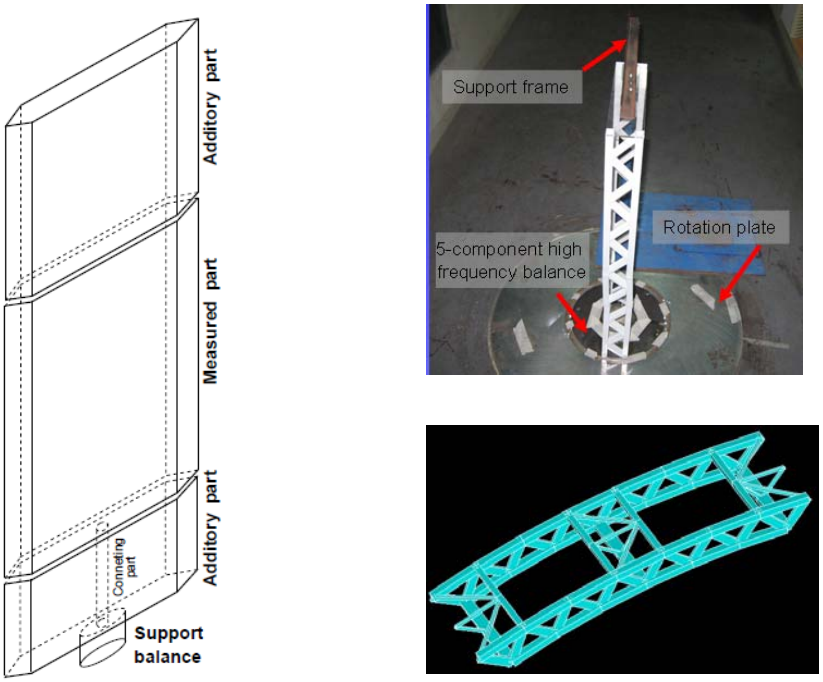

Fig. 15 Model and force-measured system in wind tunnel

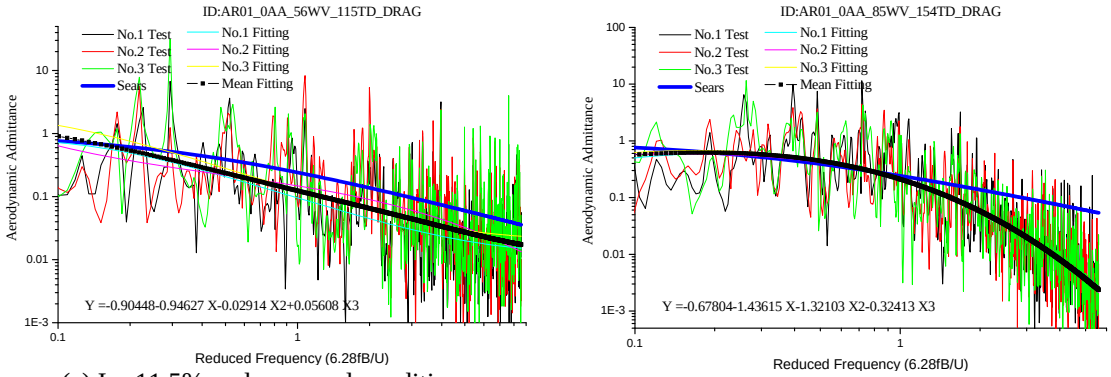

(a) Iu=11.5% under normal condition (b) Iu=15.4% under typhoon condition

Fig. 16 Equivalent drag admittance results about arch cross section

4.2 Comparison and discussion

The buffeting force is related to oncoming wind spectrum characteristics, outer shape and dynamic performance. However, during the buffeting movement, vortex-induced aerodynamic and stochastic buffeting forces are mixed between each other, not allowing for any easy division. So, the admittance function mentioned in this study includes the effect of vortex-induced force, inevitably. Based on the identified admittance function and various oncoming fluctuating wind waves for normal and typhoon conditions, numerical simulation in time domain history were carried out. In the process of computation, some effects, such as structural geometrical non-linear effects, stochastic wind angle effects from several aerodynamic loadings, such as static wind force, buffeting force, vortex-induced force and self-excited force etc. were taken into account.

For normal climate and typhoon climate, the design wind velocities at 10min time interval are 33.4 m/s and 34.9 m/s, respectively. Some more detailed information about wind field parameters are available in Table 2. In Fig. 17, the variation of wind-induced Root-Mean-Square (RMS) values relating to Xinguang Bridge under two types of climates are illustrated, in which the testing results come from measurement of full bridge aero-elastic model wind tunnel tests and the those calculated based on 1.0 admittance value and Sears function, and specified standard spectra from Chinese Loading Codes were adopted.

By comparison about several curves in Fig. 17, we know that wind-excited measured response are all obviously less than computation results. The main arch lib of Xinguang Bridge belongs typical steel-lattice structure, quite different from streamline thin-foil section. So, it is conjectured that the large difference of numerical computation from those measured may come from the selection of aerodynamic admittance function. Considering that main difference from turbulent intensity in 2-D sectional model under typhoon and normal climates, and the lateral movement in mid-span main arch of Xinguang Bridge are predominant, based on consideration of equivalent drag admittance fitting expressions (Eqs. (20)-(22)) identified under two climate turbulent fields, the process of numerical analysis were carried out again, in which the 15% standard deviation about identification results of admittance function were considered, and the confidence interval about computation results were illustrated in Figs. 18 and 19.

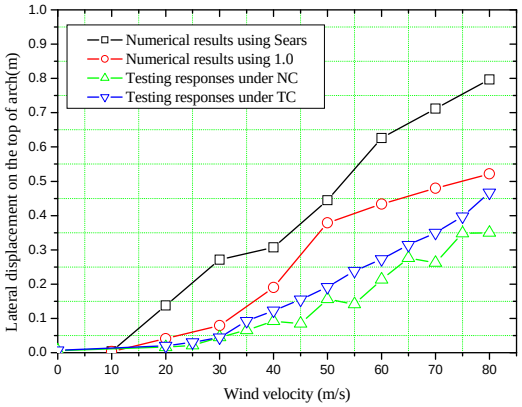

Fig. 17 Measured and computed RMS values under two climates

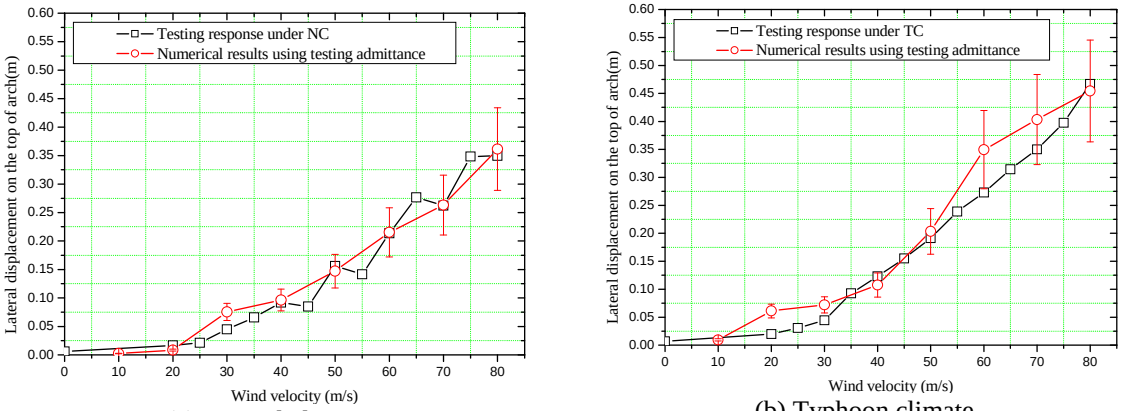

(a) Normal climate (b) Typhoon climate

Fig. 18 Measured and computed response considering admittance modification

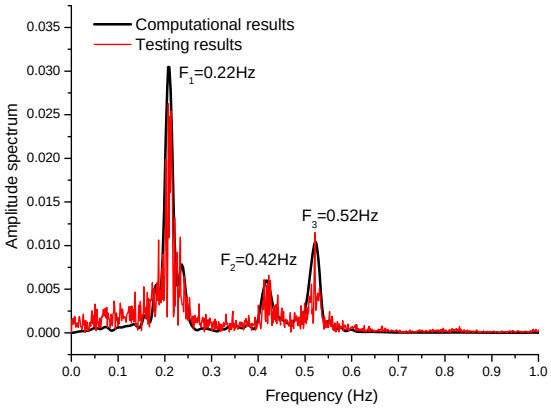

Fig. 19 Measured and computed amplitude spectrum curves

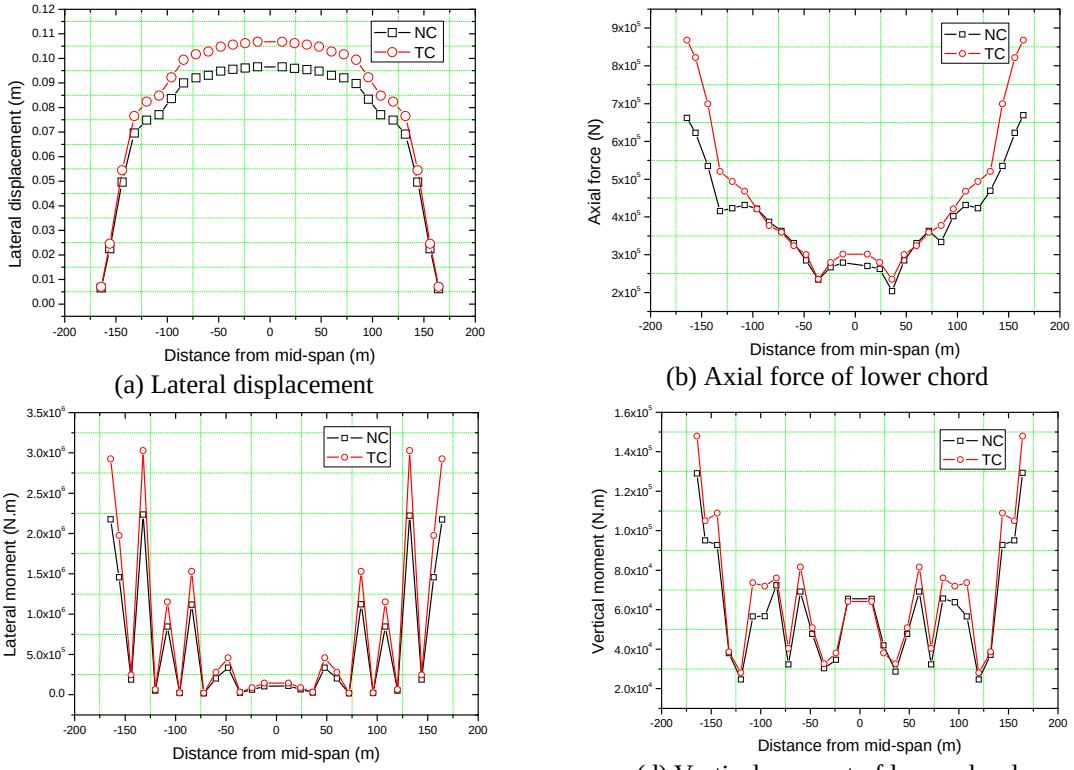

(a) Lateral displacement (b) Axial force of lower chord

(c) Lateral moment of lower chord (d) Vertical moment of lower chord

Fig. 20 Wind-induced RMS responses in mid-span arch under two climates

Once introducing the identified admittance functions, computation curves agree well with the testing measurement. From the above analysis process, it's clear that the measured admittance function can greatly improve the precision of wind-excited response. In Fig. 19, the total wind-induced response consists of three order natural modes, in which the first order symmetric lateral bending (0.22 Hz) and Second order antisymmetric lateral bending (0.42 Hz) of main arch are more than 80% of resonant fluctuation, and the rest comes from first order symmetric vertical bending (0.52 Hz) of main girder and arch, see in Table 4.

For the first symmetrical lateral bend reduced frequency under the design basic wind velocity, measured equivalent admittance value under normal climate is 0.11±0.017 (see Fig. 16(a)), while under typhoon climate mode, the corresponding value is 0.19±0.029 (see Fig. 16(b)), analytical Sears function is 0.23, and the measured admittance values are less than Sears function, say nothing of 1.0 admittance value. So, this analytically explains why there are quite larger errors between simple calculation using 1.0 or Sears admittance function and measured results in wind tunnel, in Fig. 17. Using identified admittance function, wind-induced displacement and internal-force along mid-span arch lib under two types of climate for 100 years return period design wind velocity were further compared in Fig. 20, including lateral displacement RMS in mid-span arch, axial force, lateral and vertical moment in lower chord in mid-span arch lib. For

Xinguang arch bridge, the wind-induced response under typhoon climate is greater than normal climate. Maximal wind-excited displacement response locates on the top of arch lib in the mid-span along the lateral direction, and axial force and lateral moment in lower chord in mid-span arch lib are also dominated. Maximal internal force combination appears nearby the foot of arch lib, see Fig. 20.

5. Conclusions

Based on Monte-Carlo simulation and on-site observation calibration of field parameters under typhoon condition, some basic typhoon field characteristics, including design wind velocity, average wind and turbulence intensity profiles, are qualitatively illustrated in Guangzhou region. In order to evaluate the stochastic dynamic action on flexible bridges during typhoon passages, Xinguang long-span arch bridge nearby Guangzhou downtown is selected to conduct serial case study analysis. For lattice arch cross section of Xinguang Bridge, admittance function about 2-D arch lib section is identified, then full bridge aero-elastic model tests are carried out in TJ-3 wind tunnel under two climate modes. Moreover, wind-excited response was computed considering some structural and aerodynamic nonlinearity under normal and typhoon climates, some conclusion can be reached:

- The design wind loads in typhoon-prone regions are dominated by strong typhoon, and it's necessary to carry out corresponding investigation for the typhoon field characteristics, especially, wind spectrum functions and higher turbulent intensity.
- Wind field parameters under normal and typhoon climates have larger difference, and design wind velocities are dominated by terrain topography, height from the ground and climate modes. Due to the absence of corresponding items under typhoon climate, alternative procedures simply using field parameters under normal climate would means larger error from reality.
- Since the traditional admittance treatment, such as analytical Sears function or 1.0, may over- or under-estimate wind-induced response, and admittance function depends on flow turbulence intensity for two types of climate mode, it's necessary to utilize measured admittance function based on wind tunnel tests to improve prediction precision about wind-excited performance.

Acknowledgments

The authors gratefully acknowledge the support of National Key Basic Research Program of China (i.e.973 Program) (2013CB036300), Ministry of transport application foundation research project (2013319822070) and the National Natural Science Foundation of China (91215302, 51222809 and 51178353), and the support of Program for New Century Excellent Talents in University. The dedication and efforts of postgraduate students, B. Chen, H.G. Yu, P.F. Li, and Z.X. Zai, are highly appreciated.

References

Amano, T., Fukushima, H., Ohkuma, T., Kawaguchi, A. and Goto, S. (1999), "The observation of typhoon winds in Okinawa by Doppler sodar", *J. Wind Eng. Ind. Aerod.*, **83**(1-3), 11-20.

Campbell, S., Kwok, K.C.S. and Hitchcock, P.A. (2005), "Dynamic characteristics and wind-induced response of two high-rise residential buildings during typhoons", *J. Wind Eng. Ind. Aerod.*, **93**(6), 461-482.

Deodatis, G. (1996), "Simulation of ergodic multivariate stochastic processes", *J. Eng. Mech. - ASCE*, **122**(8), 778-787.

Ding, Q.S., Zhu, L.D. and Xiang, H.F. (2011), "An efficient ergodic simulation of multivariate stochastic processes with spectral representation", *Probabilist. Eng. Mech.*, **26**(2), 350-356.

Eamon, C.D., Fitzpatrick, P. and Truax, D.D. (2007), "Observations of structural damage caused by Hurricane Katrina on the Mississippi Gulf Coast", *J. Perform. Constr. Fac.*, **21**(2), 117-127.

FEMA. (2003), *HAZUS-MH MR1: Technical Manual*, U.S.A.

Ge, Y.J. and Xiang, H.F. (2002), "Statistical study for mean wind velocity in Shanghai area", *J. Wind Eng. Ind. Aerod.*, **90**(12-15), 1585-1599.

Jakobsen, F. and Madsen, H. (2004), "Comparison and further development of parametric tropical cyclone models for storm surge modelling", *J. Wind Eng. Ind. Aerod*., **92**(5), 375-391.

Jain, A., Jones, N.P. and Scanlan, R.H. (1996), "Coupled flutter and buffeting analysis of long-span bridges", *J. Struct. Eng. - ASCE*, **122**(7), 716-725.

John, Z.Y. and Chou, C.R. (2001), "A study of the characteristic structures of strong wind", *Atmospheric Res.*, **57**(3), 151-170.

Li, Q.S., Xiao, Y.Q., Wong, C.K. and Jeary, A.P. (2004), "Field measurements of typhoon effects on a super tall building", *Eng. Struct.*, **26**(2), 233-244.

Li, Q.S., Xiao, Y.Q., Wu, J.R., Fu, J.Y. and Li, Z.N. (2008), "Typhoon effects on super-tall buildings", *J. Sound Vib.*, **313**(3-5), 581-602.

Li, Z.X., Chan, T.H.T. and Ko, J.M. (2002), "Evaluation of typhoon induced fatigue damage for Tsing Ma", *Eng. Struct.*, **24**(8), 1035-1047.

Ma, T.T., Zhao, L., Cao, S.Y., Ge, Y.J. and Miyagi, H. (2013), "Investigations of aerodynamic effects on streamlined box girder using two-dimensional actively-controlled oncoming flow", *J. Wind Eng. Ind. Aerod*., **122**, 118-129.

Meng, Y., Matsui, M. and Hibi, K. (1995), "An analytical model for simulation of the wind field in a typhoon boundary layer", *J. Wind Eng. Ind. Aerod.*, **56**(2-3), 291-310.

Meng, Y., Matsui, M. and Hibi, K. (1997), "A numerical study of the wind field in a typhoon boundary layer", *J. Wind Eng. Ind. Aerod.*, **67-68** , 437-448.

Mikitiuk, M. and Isyumov, N. *et al*. (1994), *The wind climate for Shanghai, PRC*, The University of Western Ontario, Engineering Science Research Report, BLWT-SS35-1994.

Namini, A.H. (1991), "Analytical modeling of flutter derivatives as finite elements", *Comput. Struct.*, **41**(5), 1055-1064.

Pande, M., Ho, T.C.E., Mikitiuk, M., Kopp, G.A. and Surry, D. (2002), "Implications of Typhoon York on the design wind speeds in Hong Kong", *J. Wind Eng. Ind. Aerod.*, **90**(12-15), 1569-1583.

Russell, L.R. (1971), "Probability distributions for hurricane effects", *J. Waterw. Harbor Coast. Eng. Div. - ASCE*, **97**(1), 139-154.

Scanlan, R.H. (1978), "Action of flexible bridges under wind, 1: flutter theory", *J. Sound Vib.*, **60**(2), 187-199.

Sharma, R.N. and Richards, P.J. (1999), "A re-examination of the characteristics of tropical cyclone winds", *J. Wind Eng. Ind. Aerod.*, **83**(1-3), 21-33.

Vickery, P.J. and Skerlj, P.F., Steckley, A.C. and Twisdale, L.A. (2000), "Hurricane wind field model for use in hurricane simulations", *J. Struct. Eng. – ASCE*, **126**(10), 1203-1221.

Xu, Y.L. and Zhan, S. (2001), "Field measurements of Di Wang Tower during Typhoon York", *J. Wind Eng.*

Ind. Aerod., **89**(1), 73-93.
Yasui, H., Ohkuma, T., Marukawa, H. and Katagiri, J. (2001), "Evaluation for strong winds by typhoon simulation based on Monte Carlo Method", *J. of Wind Engineering, Proceedings of the 5th Asia-Pacific Conference on Wind Engineering*, Kyoto.
Zhao, L., Lu, A.P., Zhu, L.D., Cao, S.Y. and Ge, Y.J. (2013), "Radial pressure profile of typhoon field near ground surface observed by distributed meteorologic stations", *J. Wind Eng. Ind. Aerod.*, **122**, 105-112.
Zhao, L., Ge, Y.J. and Xiang, H.F. (2005), "Application of typhoon stochastic simulation and its extreme value wind prediction", *J. Tongji University (Natural Science)*, **33**(7), 885-901. (in Chinese)
Zhao, L., Ge, Y.J. and Xiang, H.F. (2007), "MC simulation analysis about typhoon extreme value wind characteristics in Guangzhou region", *J. Tongji University (Natural Science)*, **35**(8), 1034-1038. (in Chinese)
Zhao, L. and Ge, Y.J. (2013), "Wind induced buffeting reliability of long-span cable-stayed bridge using stochastic finite element method", *Disaster Advances*, **6** (3), 32-40.
Zhu, L.D. (2002), *Buffeting response of long span cable-supported bridges under skew winds*, Ph.D. Dissertation ,The Hong Kong Polytechnic University, Hong Kong.
Zhu, L.D., Zhao, L., Ge, Y.J. and Cao, S.Y. (2012), "Validation of numerical typhoon model using both near-ground and aerial elevation wind measurements". *Disaster Advances*, **5**(1), 14-23.

CC